

ThesisTitle

by

Daniel C. Cole

Other Degrees

A thesis submitted to the
Faculty of the Graduate School of the
University of Colorado in partial fulfillment
of the requirements for the degree of
Doctor of Philosophy
Physics Physics
2018

This thesis entitled:
ThesisTitle
written by Daniel C. Cole
has been approved for the Physics Physics

Reader1

Reader2

Date _____

The final copy of this thesis has been examined by the signatories, and we find that both the content and the form meet acceptable presentation standards of scholarly work in the above mentioned discipline.

Cole, Daniel C. (Ph.D., Physics)

ThesisTitle

Thesis directed by Dr. Scott A. Diddams

Optical frequency combs have revolutionized precision metrology by enabling measurements of optical frequencies, with implications both for fundamental scientific questions and for applications such as fast, broadband spectroscopy. In this thesis, I describe the development of comb generation platforms with smaller footprints and higher repetition rates, with the ultimate goal of bringing frequency combs to new applications in a chip-integrated package. I present two new types of frequency combs: electro-optic modulation (EOM) combs and Kerr-microresonator-based frequency combs (microcombs). First I describe the EOM comb scheme and, in particular, techniques for mitigating noise in the comb generation process, and I present the results of a proof-of-principle metrology experiment and some possible applications. Then I discuss developments in microcomb technology. I present novel ‘soliton crystal’ states, which have highly structured ‘fingerprint’ optical spectra that correspond to ordered pulse trains exhibiting crystallographic defects. These pulse trains arise through interaction of the solitons with avoided mode-crossings in the resonator spectrum. Next, I describe the direct and deterministic generation of single microresonator solitons using a phase-modulated pump laser. This technique removes the dependence on initial conditions that was formerly a universal feature of these experiments, presenting a solution to a significant technical barrier to the practical application of microcombs. I also discuss generation of Kerr combs in the Fabry-Perot (FP) geometry. I introduce a nonlinear partial differential equation describing dynamics in an FP cavity and discuss the differences between the FP geometry and the ring cavity, which is the geometry used in previous Kerr-comb experiments. Finally, I discuss a technique for reducing the repetition rate of a high-repetition-rate frequency comb, which will be a necessary post-processing step for some applications. I conclude with a discussion of avenues for future research, including the chip-integration of Fabry-Perot Kerr resonators and the use of band-engineered photonic crystal cavities to further simplify soliton generation.

Acknowledgements

The work in this thesis would not have been possible...

- Acknowledgement line 1
- Acknowledgement line 2

Contents

1	PM Pumping	1
1.1	Theoretical investigation of soliton generation with a phase-modulated pump laser	1
1.2	Spontaneous generation of single solitons using a phase-modulated pump laser	4
1.3	Soliton control using a phase-modulated pump laser	5
1.4	Subharmonic phase modulation for high repetition-rate systems	7
References		10

Figures

1.1	Energy-level diagram with a phase-modulated pump laser	1
1.2	Quasi-CW background in a PM-pumped resonator	3
1.3	Mechanism for soliton generation with a PM pump	4
1.4	Experimental setup for soliton generation with a phase-modulated pump laser	5
1.5	Spontaneous generation of solitons using a phase-modulated pump laser	6
1.6	Repetition-rate control using a phase-modulated pump laser	7
1.7	Repetition-rate switching driven by a phase-modulated pump laser	8
1.8	Subharmonic phase modulation for high repetition-rate soliton generation	9

Chapter 1

PM Pumping

This chapter discusses the direct generation and control of single solitons in optical microring resonators using a pump laser phase modulated at a frequency near the resonator's free spectral range. Based on a proposal by Taheri, Eftekhar, and Adibi in 2015 [1], these results present a promising new method for simple and deterministic generation of single solitons.

To illustrate the utility of using a phase-modulated pump laser, we first present theoretical investigations into the effect of this phase modulation (PM), and then we present experimental results on the generation and control of single solitons.

1.1 Theoretical investigation of soliton generation with a phase-modulated pump laser

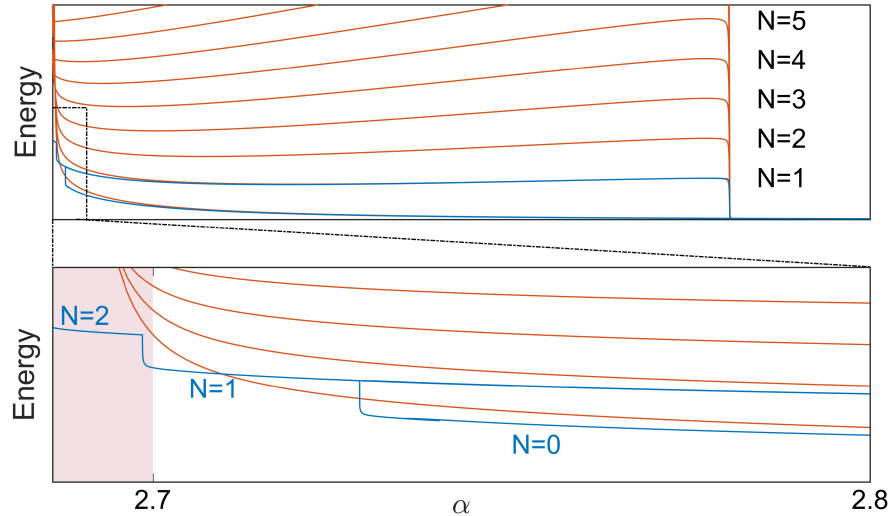


Figure 1.1: **Energy-level diagram with a phase-modulated pump laser.** An energy-level diagram with a phase-modulated pump laser (blue levels), on top of the diagram for a CW laser from Fig. ???. Phase modulation eliminates the degeneracy between the $N = 1$ level and all other levels over a range of detunings near the minimum detuning for solitons, and also precludes the existence of stable multi-soliton ensembles over the majority of the range where solitons are supported. Although the interval over which N is restricted to 1 is fairly narrow, we find that it is readily accessible in experiment. Simulations indicate that non-stationary solutions are degenerate with the $N = 2$ level for $\alpha \leq 2.7$; this region is highlighted with the red shading. The level-diagram is created using an LLE simulation with $F^2 = 4$, $\beta_2 = -0.0187$, and $\delta_{PM} = \pi$.

To theoretically explore the physics of soliton generation with PM pumping¹, we use the LLE with a modified driving term that incorporates the effect of phase modulation [1]:

$$\frac{\partial\psi}{\partial\tau}=-(1+i\alpha)\psi+i|\psi|^2\psi-i\frac{\beta}{2}\frac{\partial^2\psi}{\partial\theta^2}+Fe^{i\delta_{PM}\cos\theta}. \quad (1.1)$$

Here δ_{PM} represents the phase-modulation index, which describes the phase-modulated input field according to $E_{PM}=E_0e^{i\delta_{PM}\cos(2\pi f_{PM}t)}$; $f_{PM}\sim f_{FSR}$ is the frequency of the applied phase modulation.

Simulations of Eq. 1.1 reveal that PM transforms the resonator excitation spectrum from a series of $N=0,1,2,\dots$ up to N_{max} solitons to a single level $N=1$ near threshold, eliminating degeneracy between these states as shown in Fig. 1.1. This occurs due to spatial variations of effective loss and detuning parameters that result from the phase modulation. We can obtain an approximation for these parameters by inserting the ansatz $\psi(\theta,\tau)=\phi(\theta,\tau)e^{i\delta_{PM}\cos(\theta)}$ into the stationary ($\partial\psi/\partial\tau=0$) version of Eq. 1.1 [2]. By expanding the second-derivative term and setting derivatives of ϕ to zero we arrive at an equation for the quasi-CW background in the PM-pumped resonator:

$$F=(\gamma(\theta)+i\eta(\theta))\phi-i|\phi|^2\phi, \quad (1.2)$$

where effective local loss and detuning terms have been defined as:

$$\gamma(\theta)=1+\frac{\beta_2}{2}\delta_{PM}\cos\theta, \quad (1.3)$$

$$\eta(\theta)=\alpha-\frac{\beta_2}{2}\delta_{PM}^2\sin^2\theta. \quad (1.4)$$

This equation immediately yields an approximation for the stationary solution ψ_s :

$$\psi_s(\theta)=\frac{Fe^{i\delta_{PM}\cos\theta}}{\gamma(\theta)+i(\eta(\theta)-\rho(\theta))}, \quad (1.5)$$

where $\rho(\theta)=|\phi(\theta)|^2$ is the (smallest real) solution to the cubic polynomial that results from taking the modulus-square of Eq. 1.2:

$$F^2=\left[\gamma(\theta)^2+(\eta(\theta)-\rho(\theta))^2\right]\rho(\theta). \quad (1.6)$$

In neglecting spatial derivatives of ϕ but retaining the derivatives of the phase term $e^{i\delta_{PM}\cos\theta}$ we have made the approximation that the dominant effect of dispersion comes from its action on the existing broadband phase-modulation spectrum. This model reveals that amplitude variations in the quasi-CW background can be expected as a result of the spatially-varying effective loss and detuning terms that arise from the periodically-varying frequency of the pump laser.

Fig. 1.2 shows the predictions of simulations of Eq. 1.1 (color) and the analytical model Eq. 1.6 (black). The two agree quantitatively for weak modulation ($\delta_{PM}=\pi/2$, blue) and qualitatively with larger depth ($\delta_{PM}=4\pi$, green); both indicate that the field ψ exhibits amplitude variations due to spatially-varying effective loss and detuning. These spatially-varying parameters suggest an explanation for the spontaneous formation of a single soliton as the detuning α is decreased in terms of the local disappearance of the Kerr bistability.

As discussed in Sec. ??, for the LLE with a CW pump the background field ψ_s can take one of two stable values over a range of the parameters α and F^2 . This leads to the emergence of the ‘Kerr-tilted’ resonance like the one shown in Fig. 1.3a, with an effectively red-detuned branch lying at higher values of α , an effectively blue-detuned branch lying at lower values of α , and an interval in α over which they both exist and the system is bistable (recall that the middle branch is unstable). With spatially-varying effective loss and detuning terms, the field $\psi_s(\theta)$ described by

¹ I gratefully acknowledge the contributions of Miro Erkintalo, who originated the approximation of the derivatives of ϕ as zero and suggested the mechanism of locally-vanishing bistability for soliton generation.

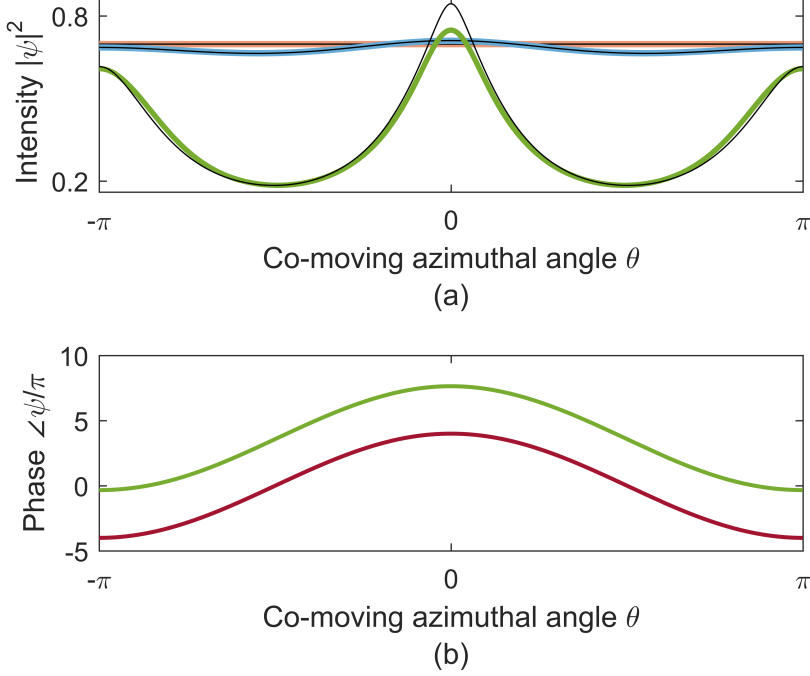


Figure 1.2: Quasi-CW background in a PM-pumped resonator. (a) Simulated intensity of the background in the resonator without (orange) and with PM of depth $\delta_{PM} = \pi/2$ (blue) and $\delta_{PM} = 4\pi$ (green), with analytical approximations in black. Here α is slightly larger than the critical value for soliton formation. (b) Phase profile of the field ψ corresponding to the green trace in (a) with $\delta_{PM} = 4\pi$, and the phase profile of the driving term $F e^{i\delta_{PM} \cos \theta}$ (red) with modulation depth 4π . The phase of the field is very nearly the phase of the drive plus a constant offset.

Eq. 1.5 now takes a value at each point in the cavity that is determined by the local parameters $\gamma(\theta)$ and $\eta(\theta)$, and it can be independently determined for each point in the cavity whether $\psi_s(\theta)$ exhibits bistability. Applying the analysis presented in Sec. ?? to Eq. 1.6, we identify the value of ρ associated with the disappearance of the bistability in a decreasing- α scan as the smaller value ρ_- at which $\partial F^2 / \partial \rho = 0$:

$$\rho_- = \left(2\eta - \sqrt{\eta^2 - 3\gamma^2} \right) / 3, \quad (1.7)$$

For fixed F^2 the function $\alpha_{crit}(\theta)$ describing the spatially-dependent disappearance of the bistability is obtained by inserting ρ_- into Eq. 1.2:

$$F^2 = \left[\gamma^2(\theta) + (\eta(\theta) - \rho_-(\theta))^2 \right] \rho_-(\theta), \quad (1.8)$$

where $\alpha_{crit}(\theta)$ is implicitly included via $\eta(\theta) = \alpha_{crit}(\theta) - \frac{\beta_2}{2} \delta_{PM}^2 \sin^2 \theta$. Fig. 1.3b shows a calculation of $\alpha_{crit}(\theta)$ for $F^2 = 4$ and $\beta = -0.0187$. For $\theta = 0$ this calculation predicts disappearance of the bistability, and subsequent soliton generation, at $\alpha = 2.741$, which is a difference of 0.4 % from the value $\alpha = 2.729$ observed in the simulation presented in Fig. 1.1. The same calculation predicts disappearance of the bistability at $\theta = \pi$ at $\alpha = 2.705$, also in close agreement with the simulation.

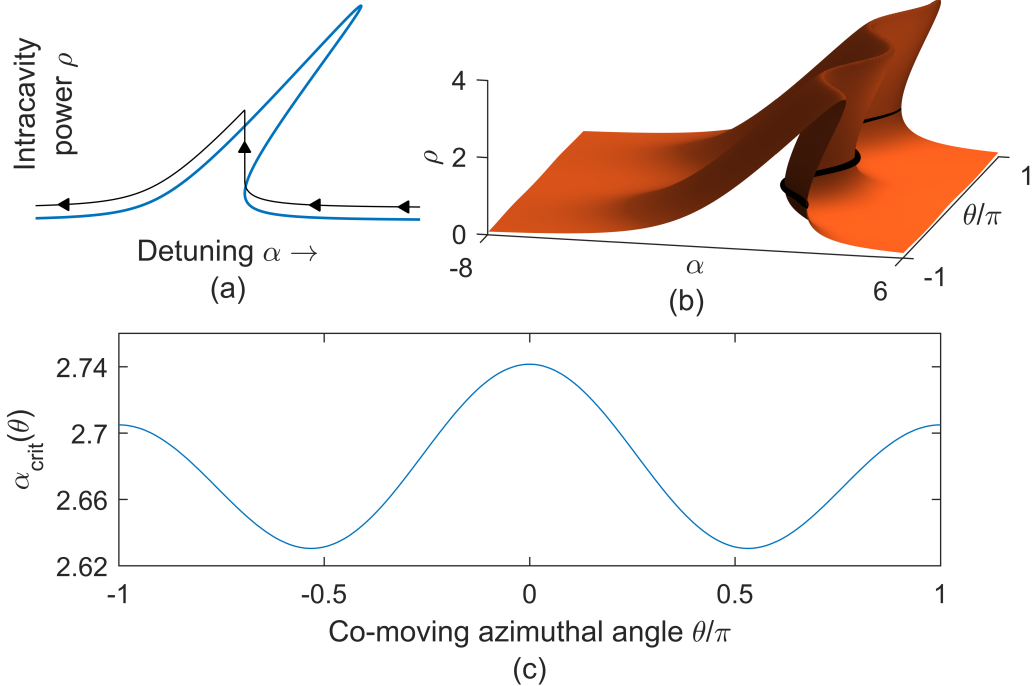


Figure 1.3: Mechanism for soliton generation with a PM pump. (a) Plot of a Kerr-shifted resonance, here with $F^2=12$. The CW background field ψ follows the black curve in an increasing-frequency scan of the pump laser. (b) For the case of a phase-modulated pump, the field $\psi_s(\theta)$ lies at a point on a qualitatively similar resonance that is defined locally by $\gamma(\theta)$ and $\eta(\theta)$ for each point θ in the co-moving frame. This plot depicts the resonance surface for $F^2 = 4$, $\beta = -0.0187$, and with $d_{PM} = 4\pi$ chosen to accentuate the θ -dependent variations in the resonance curve. The curve $\alpha_{crit}(\theta)$ is shown in black. (c) A plot of the value $\alpha_{crit}(\theta)$ at which the Kerr bistability locally vanishes and the field $\psi_s(\theta)$ must jump to the effectively blue-detuned branch, associated with the vertical transition in (a), for $F^2 = 4$, $\beta = -0.0187$, and $\delta_{PM} = \pi$. The value $\alpha_{crit}(\theta = 0)$ can be used to approximate the detuning at which a soliton is generated in an increasing-frequency scan of the pump laser, and the parameters here match the level diagram in Fig. 1.1.

1.2 Spontaneous generation of single solitons using a phase-modulated pump laser

We demonstrate deterministic generation of single solitons without condensation from an extended pattern in a 22-GHz FSR silica micro-disk resonator with $\Delta\nu \sim 1.5$ MHz linewidth [5]. We generate a frequency-agile laser for pumping the resonator by passing a CW seed laser through a single-sideband modulator that is driven by a voltage-controlled oscillator (VCO) [6]; the seed laser is extinguished in the modulator and the resulting sideband can be swept by adjusting the voltage applied to the VCO; sweeping rates up to 100 GHz/ μ s over a range over 4 GHz are possible. The pump laser is phase-modulated with index $\delta_{PM} \sim \pi$ and amplified to normalized power F^2 between 2 and 6. We are able to measure and control the pump-laser detuning in real time using an AOM-shifted probe beam as shown in Fig. 1.4, which allows thermal instabilities associated with the red detuning that is required for soliton generation to be overcome.

To generate single solitons, we begin with large red detuning $\nu_0 - \nu_{pump} = 40$ MHz and decrease the detuning until a soliton is generated near $\nu_0 - \nu_{pump} \sim 5$ MHz detuning; this value depends on the pump power and coupling condition. We measure the power converted by the Kerr nonlinearity

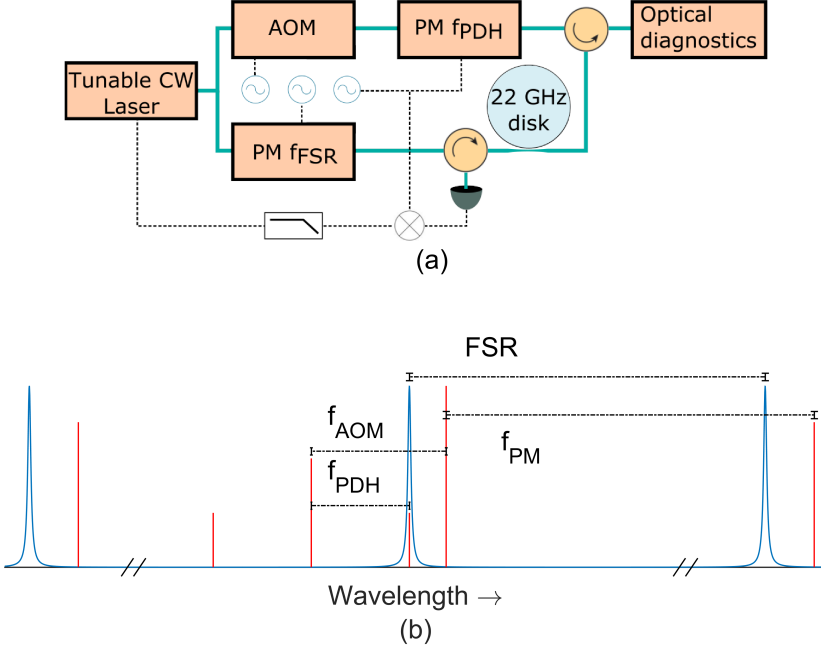


Figure 1.4: **Experimental setup for soliton generation with a phase-modulated pump laser.** (a) Schematic diagram of the experimental setup, including the pump laser phase-modulated at frequency $f_{PM} \sim f_{FSR}$ and an AOM-shifted probe beam that is modulated at frequency f_{PDH} for implementation of a Pound-Drever-Hall sideband lock. The probe beam addresses the resonator in the counter-propagating direction. (b) Frequency-domain diagram of the scheme used to maintain stable red detuning of the pump laser. As f_{PDH} is increased, the detuning α is decreased.

to new frequencies by passing a portion of the resonator's output through an optical band-reject filter; this ‘comb power’ measurement reveals a step upon soliton formation, as shown in Fig. 1.5a. After soliton generation, we observe that the soliton can be preserved while the detuning is increased again, consistent with Fig. ???. Additionally, we observe that it is possible to turn off the phase modulation without loss of the soliton, in agreement with the simulations presented in Ref. [1].

Automating soliton generation by repeatedly scanning the laser into resonance ($\nu_0 - \nu_{pump} \sim 5$ MHz) and back out again ($\nu_0 - \nu_{pump} \sim 20$ MHz, far enough that the soliton is lost) has enabled reversible generation of 1000 solitons in 1000 trials over 100 seconds, with a measured 100 % success rate. Our probe beam allows measurement of the detuning at which soliton generation occurs, which changes little from run to run. We present a histogram of detuning measurements for the generation of 160 solitons in Fig. 1.5c.

1.3 Soliton control using a phase-modulated pump laser

In addition to enabling deterministic generation of single solitons, phase modulation of the pump laser also facilitates timing and repetition-rate control of the resulting pulse train. In our experiments, the repetition rate of the out-coupled pulse train (f_{rep}) remains locked to f_{PM} over a bandwidth of ± 40 kHz. This observation is consistent with an estimate of the locking range $\delta_{PM} \times D_2/2\pi \sim 44$ kHz that is presented in Ref. [2], where we have used the approximate value $D_2 = 14$ kHz/mode. Fig. 1.6 shows the measured repetition rate as f_{PM} is swept sinusoidally through a range of ± 50 kHz around the soliton's natural repetition rate; the repetition rate follows

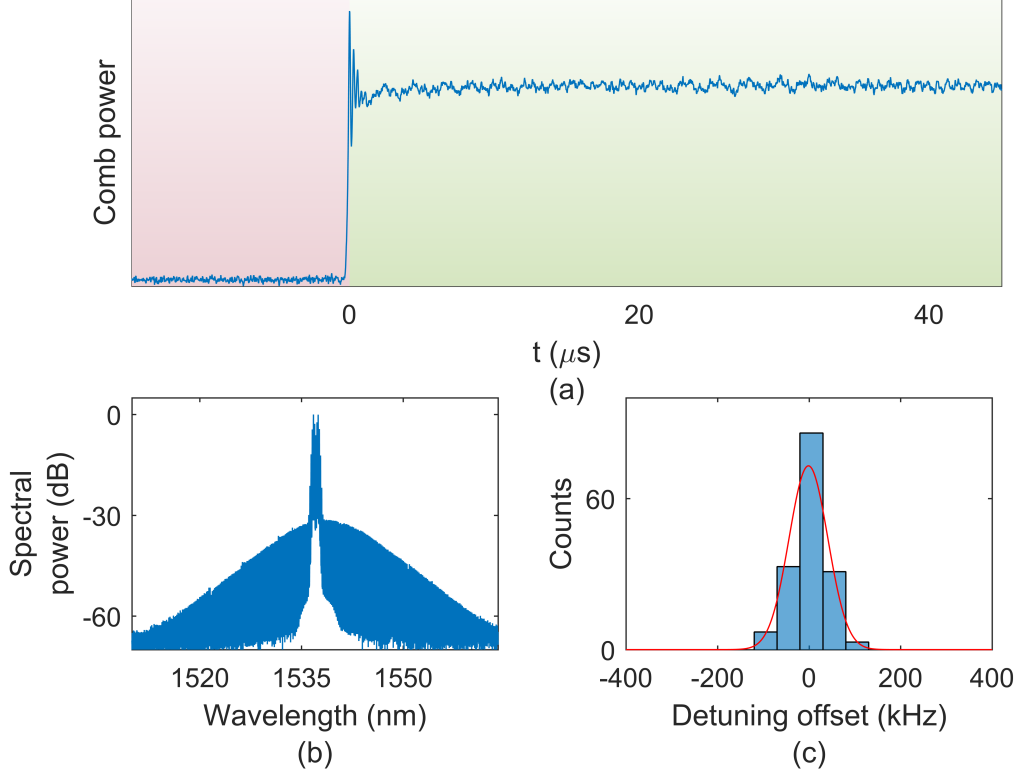


Figure 1.5: Spontaneous generation of solitons using a phase-modulated pump laser. (a) ‘Comb power’ trace obtained by filtering the pump laser out of the spectrum of light transmitted past the resonator, indicating a discrete step in the amount of frequency-converted light upon direct generation of a soliton. (b) Optical spectrum of a spontaneously generated soliton. The spectrum of the phase-modulated pump laser is visible as the set of higher-amplitude lines in the center. (c) Histogram of measured detuning values at which a soliton is generated relative to a reference (mean) value over 160 trials.

the PM except for glitches near the peaks of the sweep. In the inset of Fig. 1.6 we overlay the results of LLE simulations that qualitatively match the observed behavior. These simulations are conducted by introducing the term $+\beta_1 \frac{\partial \psi}{\partial \theta}$ to the right-hand side of Eq. 1.1, where $\beta_1 = -2(f_{FSR} - f_{PM})/\Delta\nu$ incorporates a difference between the modulation frequency and the FSR of the resonator into the model; β_1 may be varied in time to simulate the sweep of f_{PM} . These simulations indicate that the periodic nature of the glitches is due to the residual pulling of the phase modulation on the soliton when the latter periodically cycles through the pump’s phase maximum.

To evaluate the utility of phase modulation for fast control of the soliton’s properties, we measure the repetition rate of the pulse train as f_{PM} is rapidly switched by ± 40 kHz, which is within the soliton’s locking range. This measurement is conducted by photodetecting the pulse train after removing the central spectral lines corresponding to the phase-modulated pump laser using an optical band-reject filter. In order to obtain a measurement trace of the repetition rate as a function of time, the photodetected signal is split and one path is sent through a reactive circuit element (a set of low-pass filters) that induces a frequency-dependent phase shift. By comparing the phase between the two paths as a function of time, the time-dependent repetition rate can be determined.

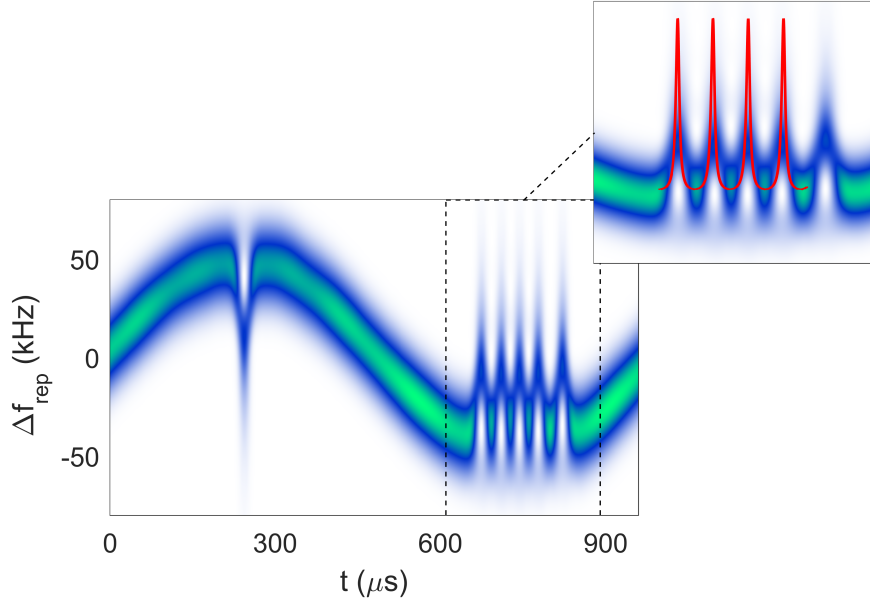


Figure 1.6: Repetition-rate control using a phase-modulated pump laser. Spectrogram of the measured repetition rate of the soliton pulse train generated by a phase-modulated pump laser as the frequency of phase modulation is swept through ± 50 kHz over 1 ms. Glitches in the spectrogram indicate that the range over which f_{rep} can be locked to f_{PM} has been exceeded. Inset: Qualitative agreement with simulations when f_{PM} is outside of the locking bandwidth, shown in red. As the soliton and the pump phase evolve at different frequencies f_{rep} and f_{PM} , the soliton periodically approaches the maximum of the phase profile. The soliton's group velocity changes, nearly locking to the phase modulation, before becoming clearly unlocked again.

We construct eye-diagrams out of the resulting data; these are shown in Fig. 1.7. In Fig. 1.7a, f_{PM} is switched with $200 \mu\text{s}$ period and $10 \mu\text{s}$ transition time; in Fig. 1.7b it is switched with $100 \mu\text{s}$ period and 60 ns transition time. These eye diagrams show that the PM enables exquisite control of the soliton pulse train.

We overlay a simulated eye diagram on the data in Fig. 1.7b. This simulation is conducted for parameters $\Delta\nu = 1.5 \text{ MHz}$, $\delta_{PM} = 0.9\pi$ that are near the experimental values, and the agreement between measurement and simulation indicates that the measurements are consistent with fundamental LLE dynamics. Fig. 1.7c presents the results of additional LLE simulations; the basic result is that the switching speed of f_{rep} is limited by the resonator linewidth, and can be only modestly improved by increasing δ_{PM} .

1.4 Subharmonic phase modulation for high repetition-rate systems

One apparent barrier to the use of a phase-modulated pump laser for protected single-soliton generation and manipulation is the electronically-inaccessible FSRs of some typical microcomb resonators. However, it is possible to overcome this challenge by phase modulating at a subharmonic of the FSR. Simulations indicate that PM can directly excite single solitons with small modulation depth, e.g. $\delta_{PM} = 0.15\pi$. In this limit, only the first-order PM sidebands are relevant, and their amplitude and phase relative to the carrier control the dynamics. For a small desired modulation depth defined by the relationship between the first-order sidebands and the carrier, it is possible to modulate at a frequency $f_{PM} \sim f_{FSR}/N$ so that the N^{th} -order PM sidebands and the carrier address resonator modes with relative mode numbers -1, 0, and 1. The depth of modulation at

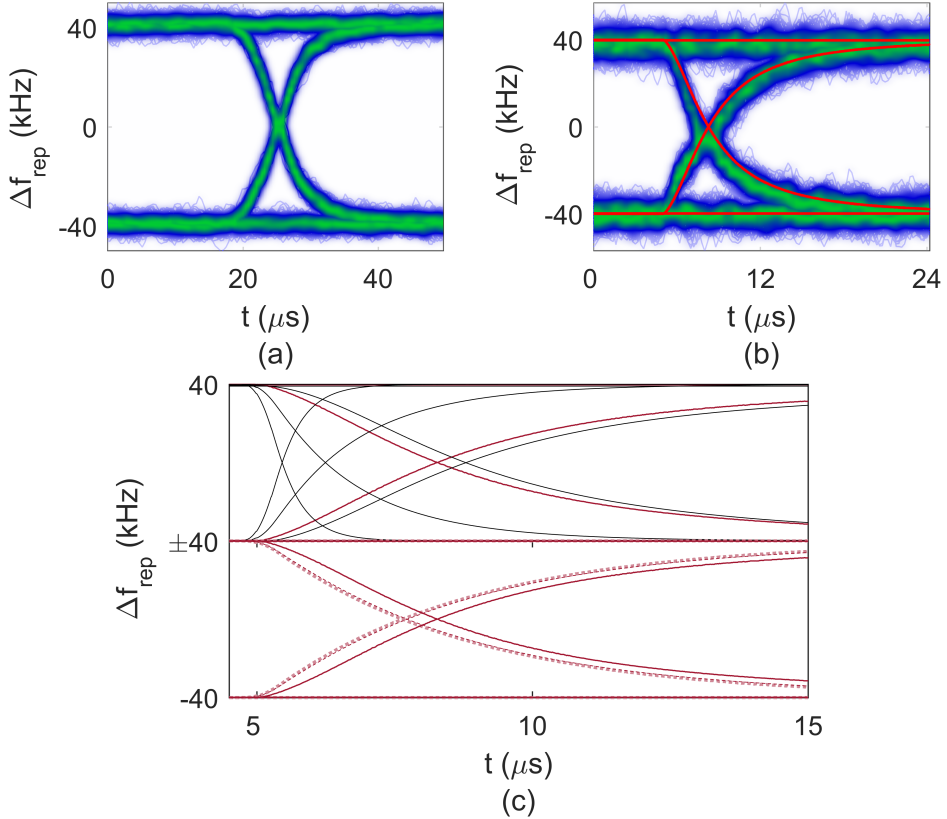


Figure 1.7: Repetition-rate switching driven by a phase-modulated pump laser. (a) Measured eye-diagram showing the switching capability of the soliton pulse train's repetition rate as f_{PM} is switched over ± 40 kHz with $10 \mu s$ transition time. (b) The same with 60 ns transition time, with an LLE simulation of the dynamics (red) overlaid. The simulation parameters are $\delta_{PM} = 0.9\pi$, $\Delta\nu = 1.5$ MHz. (c) Simulated switching dynamics for various linewidths and modulation depths. Top: $\Delta\nu=10$ MHz (fastest, left), 3 MHz, and 1.4 MHz (traces shown in solid black). Bottom: depths of 2π and 6π (dashed red, curves nearly overlap). In each, the other parameter matches the simulation in (c), which is shown again in solid red.

the frequency f_{PM} can be chosen to fix the amplitudes of the N^{th} -order PM sidebands relative to the carrier and target a desired effective modulation depth. It is worth noting that when N is odd, phase modulation is recovered when the sidebands of order $-N$, 0, and N address resonator modes -1, 0, and 1. When N is even the result is pure amplitude modulation, such that the driving term takes the form $F(1 + A \cos \theta)$. Simulations indicate that this AM profile also enables spontaneous single-soliton generation under some circumstances, but we note that this modulation profile cannot be obtained from a standard Mach-Zehnder modulator, which provides a drive like $F \cos(\eta + \delta \cos \theta)$.

Fig. 1.8 presents an example of this technique. We simulate spontaneous soliton generation with PM at $f_{PM} = f_{rep}/N = f_{rep}/21$. The effective modulation depth is 0.15π , which requires real modulation depth at the frequency f_{PM} with depth $\delta_{PM} \sim 8.3\pi$. Because the phase modulation spreads the optical power into the PM sidebands, use of this technique requires higher optical power for the same effective pumping strength; in this example the optical power must be increased by ~ 15.6 dB. A smaller real modulation depth could have been chosen to recover effective depth of $\delta_{eff} = 0.15\pi$, but our chosen depth of $\sim 8.3\pi$ gives better efficiency due to the higher ratio of the power in modes 0, ± 21 to the total power in the spectrum. While the required modulation depth and

pump power are higher with subharmonic phase modulation, neither is impractical. This technique could be used for spontaneous single-soliton generation in high-repetition rate systems; the example above indicates that it could be immediately applied in a 630 GHz-FSR resonator with 30 GHz phase modulation.

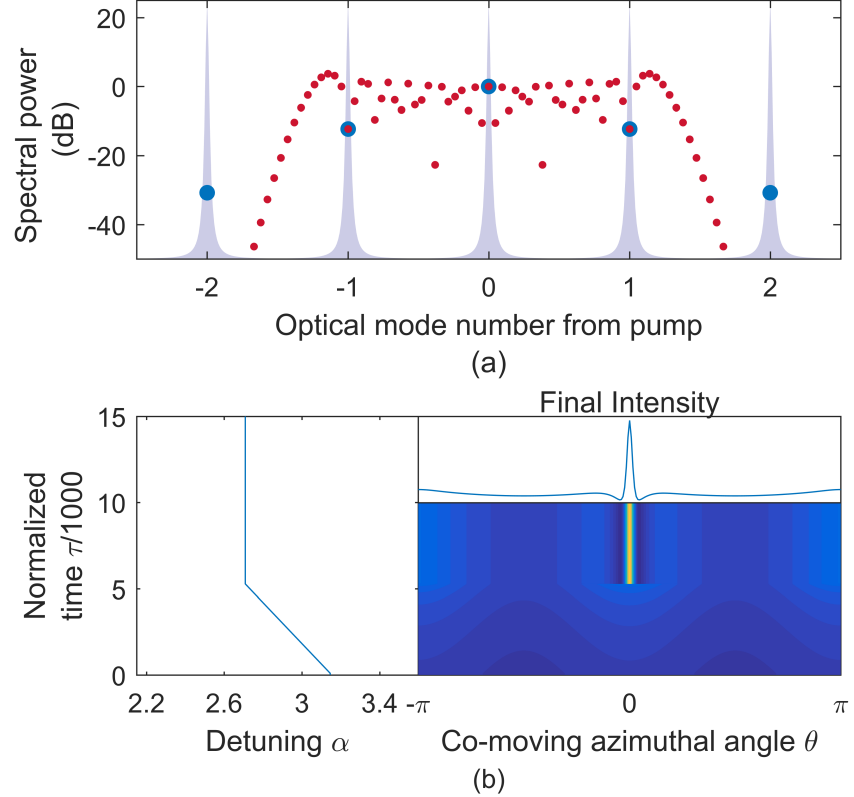


Figure 1.8: Subharmonic phase modulation for high-repetition-rate soliton generation.
(a) Spectra of PM at f_{FSR} with depth 0.15π (blue) and at $f_{FSR}/21$ with depth $\sim 8.3\pi$ (red). The relationships between the fields that address resonator mode numbers -1 , 0 , and 1 (as indicated by the gray Lorentzian curves) are the same in both cases. (b) LLE simulation of single-soliton generation using the subharmonic phase-modulation spectrum shown in red in panel (a). Only modes $n = 0, \pm 21, \pm 42, \dots$ of the phase-modulated driving field are coupled into the resonator and affect the LLE dynamics, with modes $|n| > 21$ having negligible power. As α is increased from a large initial value, a soliton is spontaneously generated, exactly as in the case of phase modulation near the FSR.

References

- [1] H. Taheri, A. A. Eftekhar, K. Wiesenfeld, and A. Adibi. Soliton formation in whispering-gallery-mode resonators via input phase modulation. *IEEE Photonics Journal*, 7 (2), **2015**, 2200309. DOI: 10.1109/JPHOT.2015.2416121 (cited on pages 1, 2, 5).
- [2] J. K. Jang, M. Erkintalo, S. Coen, and S. G. Murdoch. Temporal tweezing of light through the trapping and manipulation of temporal cavity solitons. *Nature Communications*, 6, **2015**, 7370. DOI: 10.1038/ncomms8370. arXiv: 1410.4836 (cited on pages 2, 5).
- [3] D Ceolto, A Bendahmane, J Fatome, G Millot, T Hansson, D Modotto, S Wabnitz, and B Kilber. Multiple four-wave mixing and Kerr combs in a bichromatically pumped nonlinear fiber ring cavity. *Optics Letters*, 41 (23), **2016**, 5462–5465.
- [4] Y. Wang, B. Garbin, F. Leo, S. Coen, M. Erkintalo, and S. G. Murdoch. Writing and Erasure of Temporal Cavity Solitons via Intensity Modulation of the Cavity Driving Field. *arXiv*, **2018**, 1802.07428. arXiv: 1802.07428.
- [5] H. Lee, T. Chen, J. Li, K. Y. Yang, S. Jeon, O. Painter, and K. J. Vahala. Chemically etched ultrahigh-Q wedge-resonator on a silicon chip. *Nature Photonics*, 6 (6), **2012**, 369–373. DOI: 10.1038/nphoton.2012.109. arXiv: 1112.2196 (cited on page 4).
- [6] J. R. Stone, T. C. Briles, T. E. Drake, D. T. Spencer, D. R. Carlson, S. A. Diddams, and S. B. Papp. Thermal and Nonlinear Dissipative-Soliton Dynamics in Kerr Microresonator Frequency Combs. *arXiv*, **2017**, 1708.08405. URL: <http://arxiv.org/abs/1708.08405>. arXiv: 1708.08405 (cited on page 4).
- [7] J. Hult. A Fourth-Order Runge-Kutta in the Interaction Picture Method for Simulating Supercontinuum Generation in Optical Fibers. *Journal of Lightwave Technology*, 25 (12), **2007**, 3770–3775. DOI: 10.1109/JLT.2007.909373.
- [8] A. M. Heidt. Efficient Adaptive Step Size Method for the Simulation of Supercontinuum Generation in Optical Fibers. *Journal of Lightwave Technology*, 27 (18), **2009**, 3984–3991.
- [9] G. P. Agrawal. **Nonlinear Fiber Optics**. 4th. Burlington, MA: Elsevier, 2007.
- [10] M. Hirano, T. Nakanishi, T. Okuno, and M. Onishi. Silica-Based Highly Nonlinear Fibers and Their Application. *Sel. Top. Quantum Electron.*, 15 (1), **2009**, 103–113. DOI: 10.1109/JSTQE.2008.2010241.
- [11] K. J. Blow and D Wood. Theoretical description of transient stimulated Raman scattering in optical fibers. *Quantum Electronics, IEEE Journal of*, 25 (12), **1989**, 2665–2673. DOI: 10.1109/3.40655.